Computers & Geosciences 91 (2016) 77–89

Contents lists available at ScienceDirect

Computers & Geosciences

journal homepage: www.elsevier.com/locate/cageo

Case study

Badlands: An open-source, flexible and parallel framework to study landscape dynamics

T. Salles *, L. Hardiman

School of Geosciences, University of Sydney, Sydney, NSW 2006, Australia

ARTICLE INFO

Article history:
Received 24 November 2015
Received in revised form
14 March 2016
Accepted 17 March 2016
Available online 19 March 2016

Keywords:
Landscape
Drainage
Climate
Delta
Numerical model
Parallel

ABSTRACT

In this paper, we propose a minimal numerical model which governing equations describe the following processes: erosion, sedimentation, diffusion and flexure. The model respects conservation laws for water and sediment. The implementation is based on a finite volume approach and the explicit solution stability is ensured by a CFL-like condition. This common core of accepted physical principles governing landscape evolution is ported into a distributed memory parallel environment. *Badlands* (acronym for *BA*sin an*D* *LAN*dscape *D*ynamic*S*) is an open-source, flexible, TIN-based landscape evolution model, built to simulate landform development and test source-to-sink concepts at regional to continental scale over thousands to millions of years. To illustrate the model capabilities, we first present an example of delta evolution under sea-level fluctuations. The model predicts the successive progradation and transgression phases, the development of depositional and erosional patterns as well as the associated stratigraphic formation. Then, we investigate the importance of climate, and in particular the spatial pattern of precipitation, on the topographic evolution of mountain belts. The simulation and associated quantitative analyses suggest that the main drainage divide migrates and asymmetric topography develops in response to orographic precipitation. This mechanism, documented in recent analogue and numerical experiments, results in a complex reorganisation of drainage networks that our model is able to reproduce.

1. Introduction

Landscape evolution models (LEMs) have allowed the geoscience community to test and develop new conceptual models and quantify the drivers and feedback mechanisms responsible for shaping the Earth's envelop (see Fig. 1). LEMs usually simulate, based on physical laws and principles, some of the fundamental geomorphological processes acting on the Earth surface and for which the driving forces, initial and/or boundary conditions are well constrained (Tucker, 2009). Most of these numerical models have been developed to address medium to large scale landscape dynamic over spatial dimensions of a catchment to an orogen and temporal dimensions of thousands to millions of years (Willgoose, 2005; Paola et al., 2009). LEMs are currently used as an aid in various research fields such as hydrology, soil erosion, hillslope stability, volcanology and general landscape evolution studies (Refice et al., 2012).

In this paper, we present our LEM *Badlands*, which is an open-source and parallel catchment and landscape model capable of simulating both erosion and deposition over time scale of thousands to millions of years and over regional to continental scale. The model source code, its associated documentation along with the input files for the examples discussed in this paper are available on Github (*http://github.com/badlands-model*). The physics of Badlands model is simpler than many other models (Coulthard, 2001; Tucker et al., 2001; Garcia-Castellanos et al., 2003; Perron et al., 2009; Braun and Willett, 2013; Goren et al., 2014; Salles and Duclaux, 2015) and therefore our goal is not to produce models with more sophisticated physics, but rather develop an efficient parallel code to model landscape dynamics problems at very high resolution.

The first objective is to present the main physical and empirical laws which are used in Badlands. The set of equations is based on the assumption of uniform substrate and no differentiation between regolith and bedrock (Braun and Sambridge, 1997; Tucker et al., 2001). The rate of river incision is described using the classical stream power equation (Howard, 1980). The hillslope processes are simulated based on a linear sediment transport law, which sets the transport flux equal to a linear function of topographic slope: the simple diffusion law (Braun et al., 2001; Sweeney et al., 2015). Modelling of the isostatic loading of the Earth's crust is performed using the approach of Li et al. (2004).

* Corresponding author.
E-mail address: tristan.salles@sydney.edu.au (T. Salles).

http://dx.doi.org/10.1016/j.cageo.2016.03.011
0098-3004/

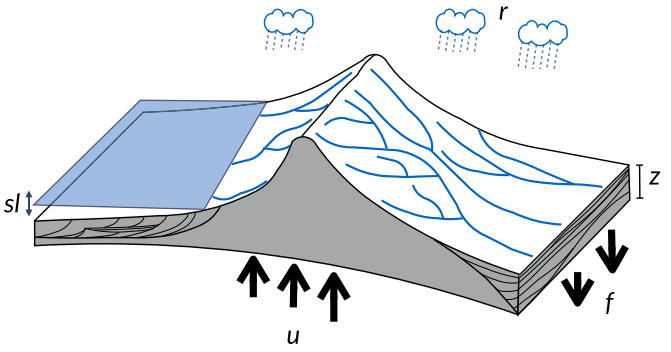

Fig. 1. A schematic of two-dimensional landscape evolution model illustrating the main variables and forces simulated with Badlands: z is the surface elevation, r refers to rainfall, sl to sea-level fluctuations, f to the flexural isostasy and u to tectonic uplift.

The method is capable of modelling both local and regional isostatic compensation. The combination of a high-order approximation scheme and a multi-grid technique (Li et al., 2004) has been modified to simulate flexure of realistic lithosphere (laterally heterogeneous).

The second objective is to describe the main characteristics of Badlands implementation. In order to avoid the limitations associated with grid-based models, the terrain surface is discretised as a set of vertices in any arbitrary configuration (Braun and Sambridge, 1997; Tucker et al., 2001). These nodes are connected to form a Delaunay triangulated irregular mesh (Shewchuk, 2002). The Delaunay framework also offers a numerical solution for the constitutive laws using finite-volume methods (Tucker et al., 2001). A forward in time explicit schema ensures stability based on a CFL-like condition (Refice et al., 2012). Key to any LEM algorithm is to order the nodes in a way that makes the computation of both discharge and sediment transport efficient. This is achieved here by implementing the single flow direction water flow routing approach of Braun and Willett (2013) which transformed this $O(n^2)$ problem into an $O(n)$ one. Finally, the algorithm is coded to take advantage of parallel architectures. The parallelisation strategy is based on sub-catchment partitioning, an approach inspired from hydrologic models (Arnold et al., 1998; Vivoni et al., 2011). The method ensures a balanced load (*i.e.*, equivalent number of nodes per processor) and a minimal number of communications (*i.e.*, data exchanges between processors and computational nodes). To illustrate the performance of our partitioning approach we monitor execution time and speed-up in a simple example of drainage evolution under uniform precipitation.

The final objective is to test our model using simple examples of the development of delta fronts and orogenic landscapes. Our goal is not to reproduce all the complexity of the natural landscape response to sea-level fluctuations and climate change, but rather to extract first-order behaviours from the set of physical equations defined in Badlands. In our first example, we monitor the impact of sea-level fluctuations on the evolution of the erosional and depositional patterns of an circular island under uniform precipitation. The simulated stratal architectures mimic the development of successive progradation and transgression phases observed on natural systems (Catuneanu, 2006). Then for the second example, the quantitative analyses focus on drainage catchments evolution and networks reorganisation induced by the migration of the main drainage divide under an imposed precipitation gradient. The interpretations and discussions focus on the evolution of the drainage catchments (Bonnet, 2009), the balance between diffusive (hillslope) and advective (channel) processes (Perron et al., 2009; Giachetta et al., 2012) and channel longitudinal evolution. The model results are in agreement with recent studies based on natural, analogue and numerical models (Willett, 1999; Bonnet, 2009; Perron et al., 2009; Giachetta et al., 2012).

2. Constitutive laws

2.1. Landscape evolution model equations

In Badlands, we assume that all sediment properties (*e.g.* composition of the solid fraction, particle size, bulk density or thermal properties) are temporally and spatially uniform and that there is no differentiation between regolith and bedrock. Under these assumptions, the continuity of mass corresponds to the interaction of three types of processes, one driven by tectonic, another describing the smoothing effects associated to diffusive processes, and a last one representing the erosive power of water flow. This standard model is of the form

$$\frac{\partial z}{\partial t} = -\nabla\cdot\mathbf{q_s} + u$$

where u in m/a is a source term that represents tectonic uplift. $\mathbf{q_s}$ is the depth-integrated, bulk volumetric sediment flux per unit width (m^2/a). The local rate of downhill sediment transport involves two possible processes (though additional processes can easily be implemented): transport by channel flow $\mathbf{q_r}$ and diffusion $\mathbf{q_d}$.

Expressions for transport by channel flow and linear diffusion are already well described in the literature (Chen et al., 2014 and references therein). The sediment transport rate per unit width by flowing water, $\mathbf{q_r}$, is modelled as a power function of topographic gradient ∇z and contributing drainage area A. Parameter A is related to surface water discharge per unit width q_w through net precipitation P, which can be uniform or spatially variable. With this formulation, A is used as a proxy for the sediment flux in a detachment-limited erosion regime.

$$-\nabla\cdot\mathbf{q_r} = -\epsilon A^m(\nabla z)^n$$

This expression corresponds to a simplified form of the usual expression of sediment transport by water flow (Howard, 1980), in which the transport rate is assumed to be equal to the local carrying capacity, which is itself a function of boundary shear stress or stream power per unit width (Tucker and Hancock, 2010). We consider additionally no threshold for particle entrainment. In addition, the parameterisation of the sediment transport includes the simple creep transport law which states that transport rate depends linearly on topographic gradient (Fernandes and Dietrich, 1997). Downslope simple creep is commonly regarded as operating in a shallow superficial layer (Braun et al., 2001)

$$-\nabla\cdot\mathbf{q_d} = -\kappa\nabla^2 z$$

The coefficients κ and ϵ are scale-dependent (Dietrich et al., 1995) and their values depend on lithology and mean precipitation rate (Whipple and Tucker, 1999), channel width, flood frequency, channel hydraulics, and potentially other parameters and processes (Lague et al., 2005). The coefficients m and n are positive constants which depend generally on the erosion process being simulated. The values of m and n indicate how the incision rate scales with bed shear stress for constant value of sediment flux and sediment transport capacity. There are no universal values of m and n. Generally, m and n are both positive, and their ratio (m/n) is considered to be $\simeq$0.5, in which case $A^m(\nabla z)^n$ scales with shear stress to a positive power (Tucker and Hancock, 2010).

2.2. Flexural isostasy

Flexure of the lithosphere is a process by which loads bend the

elastic outer shell of the Earth. As opposed to hydrostatic approaches, flexural models assume that the lithosphere is a composite layered body, where the upper crust is similar to an elastic plate while the lower crust and upper mantle behave as a viscous fluid.

The equations governing elastic deformation are given by

$$D\nabla^2\nabla^2\omega + \Delta\rho g\omega = q_l$$

where ω is the vertical deflection of the plate and $\Delta\rho = \rho_m - \rho_f$ is the density difference between the mantle and the filling material (either sediments, air or water or a combination of both). q_l is the net force per unit area exerted by the applied load, $q_l = \rho_l g h_l$, ρ_l and h_l are the density and height of the load, respectively; g is the gravitational acceleration.

D is the flexural rigidity of an elastic plate

$$D = \frac{ET_e^3}{12(1-\nu^2)}$$

where E is Young's modulus, ν is Poisson's ratio and T_e is the effective thickness of the elastic plate. In Badlands, the effective thickness T_e could vary in space making it possible to study non-homogeneous plate response to differential loading.

The above equations are linearisable, and therefore can be solved by superposition of analytical solutions (Wickert, 2015 and references therein). Here, a different technique based on multi-grid solutions to the biharmonic equation adapted from Altas et al. (1998) and proposed by Li et al. (2004) is implemented. The approach guarantees convergence and has the advantage of dramatically reducing the computational cost. As shown in Li et al. (2004), the technique is capable of simulating both local and regional isostatic compensation. Compared with other isostatic models, it is more robust and computationally efficient.

The elastic deformation solution is solved with a fourth-order finite difference approximation schema. The convergence is ensured by smoothing oscillating error using a multi-grid technique in which the solution is iteratively computed by travelling up and down the grid hierarchy. Similar to Li et al. (2004), three grids are used to get a fast convergence rate using a *V-cycle* scheme. At the four boundaries of a rectangular simulation area, the gradients of the deflection are set to zero (free boundary condition).

Left side of Fig. 2 presents the resulting homogeneous plate deflection under a 100 km wide and 50 m tall sediment load. For a continuous plate with a load of finite width, an analytic solution was derived by using Green's function (Slingerland et al., 1994) and is plotted over the model results showing good agreement between the approach and the analytical solution. Right side plots show the response to a 100 km wide, 300 m height central circular sedimentary load for both homogeneous and non-homogeneous (bottom plot) plate.

3. Implementation

3.1. Spatial and temporal discretisation

Badlands uses an irregular spatial discretisation scheme to solve the geomorphic equations (Braun and Sambridge, 1997). The computational mesh is created using *Triangle* library from Shewchuk (2002). From a series of regularly spaced coordinates, a set of irregular points is generated which are connected using a Delaunay triangulation (Voronoi, 1908; Delaunay, 1934) to form a triangulated irregular network (TIN). *Triangle* generated scattered points ensures that the created TIN resolution matches the user-defined one. It is also possible to specify regions of different resolutions within the overall simulated domain.

Following Tucker et al. (2001), the dual Delaunay–Voronoi framework could be used to solve the continuity equation using a finite volume approach. Applying the divergence theorem for a considered node i the flux to node j is positive if the net sediment flux is from i to j, and negative otherwise. The finite volume approach is conservative (*i.e.*, the flux entering (or leaving) a given cell equals the flux leaving (or entering) the adjacent cell). The integration of the conservation equation for node i is written as

$$\frac{dh}{dt} = u - \frac{1}{\Omega_i}\left(\sum_{j=1}^{n_i} w_{ij} q_{s,ij}\right)$$

where n_i is the number of natural neighbours connected to node i, w_{ij} is the width of the edge shared by adjacent Voronoi cells associated to the node i and its neighbour j, and $q_{s,ij}$ is the total volumetric sediment flux across this edge per unit width.

The irregular nature of the grid prevents water-flow directional bias that arises in regular grids, and allows for a 3-D advection of the nodes due to complex tectonic displacements. Within Badlands, one can control the density of the TIN nodes and automatically adjust the TIN resolution based on areas showing rarefaction or accumulation of nodes. The *Triangle*'s library ensures that the newly advected TIN is a constrained Delaunay that (1) prevents the occurrence of low node density areas and (2) enforces the required resolution for surface processes. In addition, a node deletion/merging algorithm has been implemented to circumvent the problem of progressive increase of node number density which could lead to significant slowdown of the surface process model. The criteria for deletion and merging are based on the distance between neighbouring nodes and the minimal interior angle of each Delaunay triangulation.

Using an explicit time integration scheme, the length of the time steps is determined by using a Courant–Friedrichs–Lewy (CFL) like condition in order to ensure numerical stability. To this end, each of the two processes provides an upper time step limit. The minimum among the CFL limits returned is then used as time step for the next iteration. Following Refice et al. (2012), the time step limit is given by

$$\Delta t_{max} < \min_{i,j}\left[\left(\frac{l_{ij}^2}{2\kappa}\right), \left(\frac{l_{ij}}{\epsilon q_{w,i}^m (\nabla z_{i,j})^{n-1}}\right)\right]$$

where l_{ij} is the TIN arc length, with themin being calculated over all the TIN arcs.

3.2. Ordering and partitioning

To solve channel incision and landscape evolution a key component in the algorithm consists in finding as efficiently as possible the order in which one must go through the nodes to compute discharge and sediment transport progressively. In Badlands, the $O(n)$-efficient ordering method from Braun and Willett (2013) is implemented. The technique is based on a single-flow-direction (SFD) approximation assuming that water goes down the path of the steepest slope (O'Callaghan and Mark, 1984; Gallant and Wilson, 2000). The algorithm consists first in defining the receivers list (a receiver of a given node is its neighbour with the lowest elevation), then by inverting the list of receivers to obtain the donors list. After what a stack is created starting from any base level nodes (*e.g.* a node which is his own receiver) and adding recursively their corresponding donors until a node with no donors is reached. The obtained stack contains all the nodes belonging to the catchment of a considered base level nodes. After inverting the stack, the resulting order of the nodes is such that, within each catchment, all nodes upstream of a given node are processed before the inverted stack proceeds downstream.

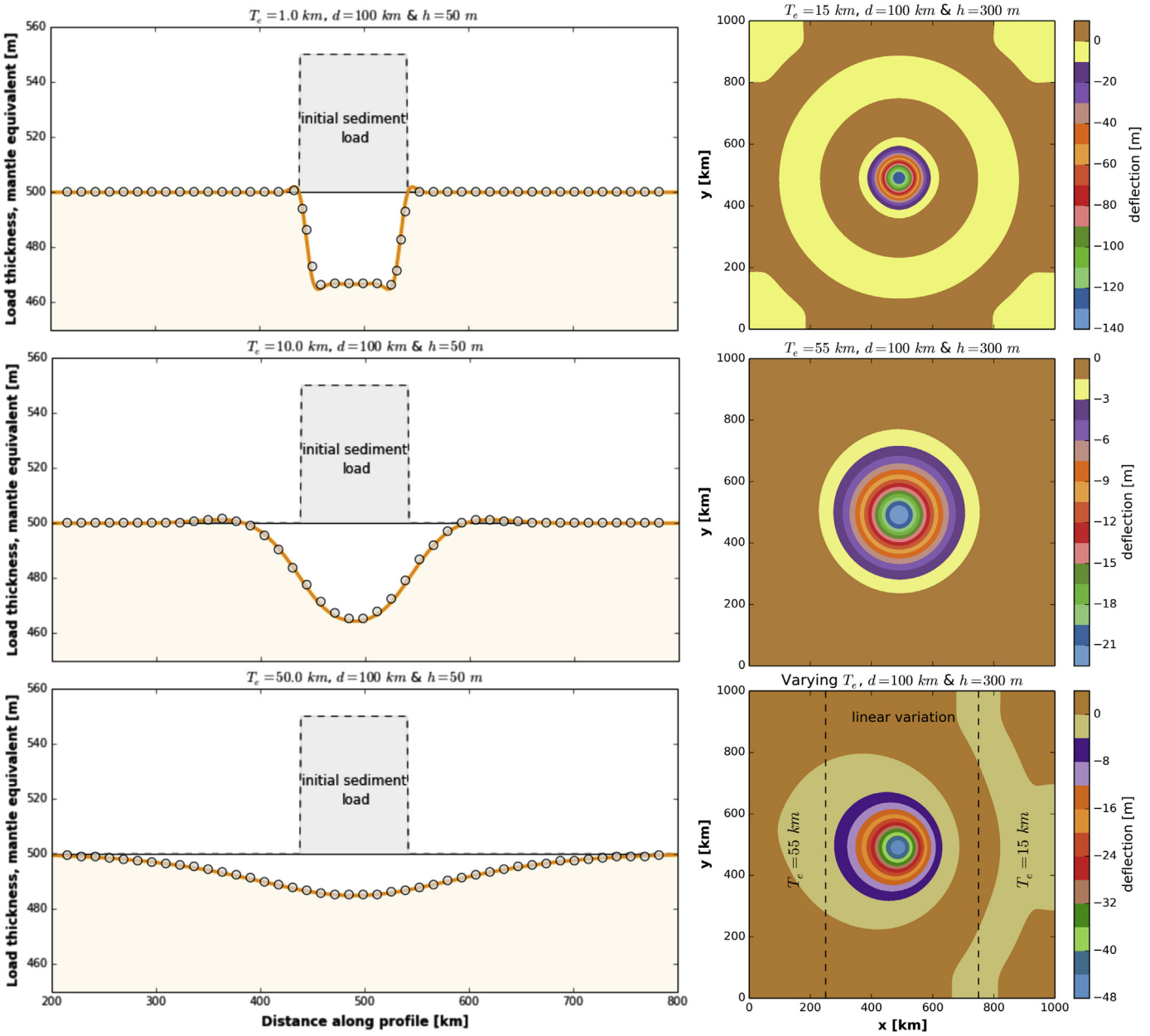

Fig. 2. Left graphs: numerical solutions in response to a 100 km-long and 50 m height central line sedimentary load. Deflection curves calculated for different elastic thicknesses: (top) 1 km, (middle) 10 km and (bottom) 50 km. Orange curves show Badlands' results; superimposed circle marks are the results from Slingerland's model. Right plots: 2-D numerical solutions in response to a 100 km-in-diameter, 300 m height central circular sedimentary load. Plots showing resulting deflection due to uniform elastic thickness of 15 km (top) and 55 km (middle) as well as for a linearly varying elastic thickness (bottom). (For interpretation of the references to colour in this figure caption, the reader is referred to the web version of this paper.)

The method proposed above can be implemented to take advantage of parallel architecture as proposed in Braun and Willett (2013). However their parallelisation approach, which is based on catchment partitioning, needs to be improved for better performance. The first problem with their approach is that the number of catchments in a given simulation will limit the number of computational cores that could be used efficiently. The second, more problematic, is that most catchments have varying number of nodes. The computational effort (diffusion and stream power law) in a given catchment is determined mainly by the number of nodes retained in the TIN and the catchment size. Therefore splitting processors by catchment will result in most cases in unbalanced simulations.

To circumvent these problems, the approach implemented in Badlands consists in splitting each of the catchments into numerous sub-catchments (see Fig. 3a). From the ordering method, the channel network could be seen as an acyclic, directed graph, such that reaches and junctions are ordered from upstream to downstream direction (as shown in Fig. 3b). Individual sub-catchments draining to channel reaches form the basis for partitioning the simulated area into smaller units and synchronising effort in an upstream to downstream order. This approach is commonly applied in hydrologic models to divide a large river catchments into simpler units (Arnold et al., 1998). As the landscape evolution calculations are organised according to channel reaches, the parallelisation strategy follows the natural river catchments organisation with information on sediment fluxes being passed between sub-catchments in a sequential fashion at each time step (Fig. 4a). The computational effort in a sub-catchments is determined by the number of nodes retained in the TIN

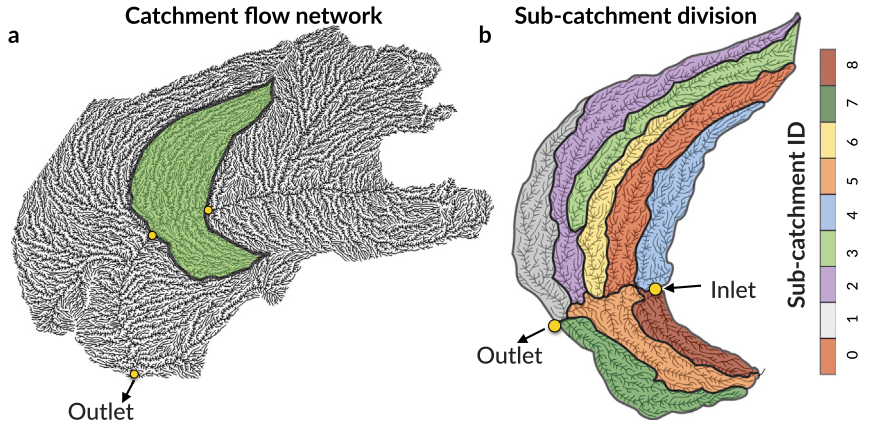

Fig. 3. Sub-catchment delineation allows partitioning a 74,000 nodes TIN domain into smaller units of variable size connected via the channel network. (a) shows an entire catchment based on its stream network. A small portion of the catchment (green area) is presented in (b) and illustrates the result from the division in 9 sub-catchment units. (For interpretation of the references to colour in this figure caption, the reader is referred to the web version of this paper.)

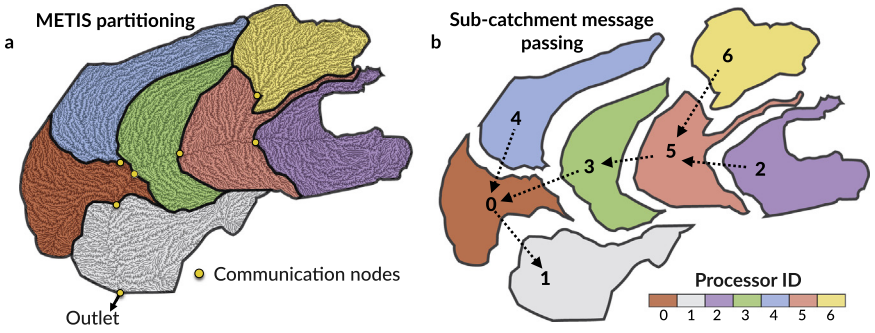

Fig. 4. Illustration of the partitioning strategy implemented in Badlands showing in (a) the distribution of the catchment nodes between 7 processors. This distribution is based on the stream network connectivity table that is passed to the *METIS* library. The library balances the number of nodes among processors while minimising the communications. (b) shows an hypothetical communication flux between the flow graph sub-divisions.

and the sub-catchments size. Data exchanges or message passing between sub-catchments consist of lateral sediment fluxes through the channel network in upstream to downstream order (as shown in Fig. 4b). Exchanges are performed through message passing (*MPI* Gropp et al., 1999) using ghost cells located at junctions between sub-catchments. To both balance the computational load and minimise the message passing between processors, we use the graph partitioning library *METIS* (Karypis and Kumar, 1999). The library uses a connectivity table which is derived, in our model, from Strahler stream order (Strahler, 1952) and surface water discharge.

4. Performance test

Performance tests are realised using Intel Xeon Haswell 2.6 GHz processors available from the Australian Pawsey Supercomputing Centre. Each computational node contains 12 Intel Xeon processors.

The load-balancing method using *METIS* is designed to partitioning the TIN vertices of the flow network (which could be seen as a directed graph) into roughly equal parts. Fig. 5a shows the number of nodes associated with each sub-catchment. The repartition is clearly unbalanced with some sub-catchments containing 5–6 times more nodes than others. Without applying any load-balancing technique, a direct parallelisation of this distribution might result in unscaled computational runs. Graphs (b), (c) and (d) in Fig. 5 show the resulting Badlands load balancing of the surface nodes for 3 runs with different number of processors. As the processors number increases, the number of nodes per processor decreases from more than 27,500 nodes (standard deviation: $\sigma \simeq 480$) with 40 processors to less than 5000 ($\sigma \simeq 180$) for 230 processors. The distribution of the load shows that each of the processors will contain approximately the same number of nodes. Based on the idea that the computational effort for a given model is determined, in part, by the number of nodes retained in each processor, the obtained parallel distribution will help in reducing computational time. To be efficient the partition needs not only to balance the computational load but also to minimise message passing between processors. Left graph in Fig. 6 shows, with the 2 TIN resolutions, the number of communication nodes for varying number of processors. The number of message passing through each processor is on average equal to 1 or 2 which limits the computational time inherent to inter processes communications.

Overall, the construction of the sub-catchments distribution and its partitioning based on the *METIS* library performs well for all the runs. Right graph in Fig. 6 illustrates the performance of Badlands for a given iteration step. The considered iteration consists in (1) the creation of the flow network based on the ordering algorithm, (2) computation of flow discharge and Strahler stream order, (3) sub-catchment partitioning using *METIS* library, (4) erosion, transport and sedimentation computation, (5) update of the rainfall regime and (6) parallel outputs creation. It is important to note that the chosen time step is the most time consuming as it requires an update of climatic conditions and the creation of the outputs. In Badlands, this specific time step recurrence is user defined, the outputs are written in parallel using the HDF5 library. The black curve (Fig. 6 right) shows the computational time in ms versus the number of processors. The curve drops quickly from above 18 s for 2 processors to 4.7 s for 20 processors. The curve then flattens while keeping its decreasing trend and reaches 1.1 s for 230 processors. To assess the parallel performance in a normalised fashion, we calculate the speed-up (s_u, grey curve in right graph Fig. 6). s_u is defined as the ratio of the execution time for the serial operation to

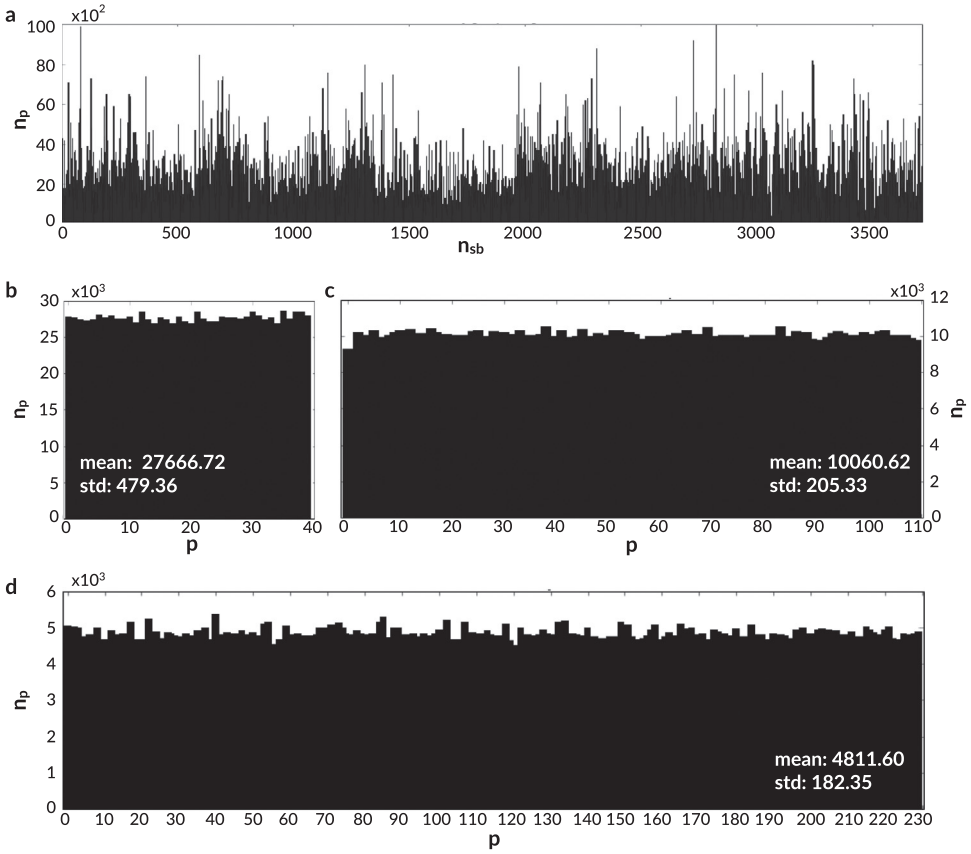

Fig. 5. (a) Distribution of nodes (n_p) per sub-catchments (n_{sb}: number of sub-catchments). Graphics (b), (c) & (d) show the number of nodes (n_p) per processor p for 3 similar simulations ran with 40, 110 and 230 processors respectively. It illustrates the node balancing resulting from Badlands partitioning method.

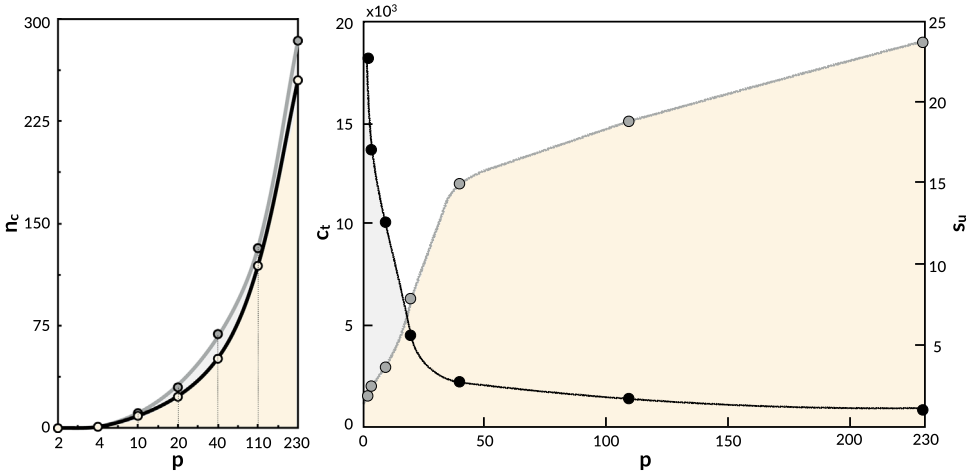

Fig. 6. Left: Results for 2 TIN resolutions (grey: $n_p > 1.1 \times 10^6$ – light orange: $n_p > 0.8 \times 10^6$) showing number of communication nodes (n_c) for the entire domain after 200,000 years of simulation for 7 models ran with 2, 4, 10, 20, 40, 110, 230 processors. Right: Black dots and curve show computational time c_t in ms for a single model iteration for different number of processors p. Speed-up, s_u, as a function of number of processors for the different simulations. (For interpretation of the references to colour in this figure caption, the reader is referred to the web version of this paper.)

the execution time for the parallel operation with p processors. In an ideal situation, $s_u = p$, implying that the speed-up grows at the same rate at which processors are added to the parallel operation. For this experiment, the speed-up attains values ranging from 2 to 24, indicating that the parallel model is 2–24 times faster than the serial version. Parallel speed-up improves with the number of processors and nodes, with models' performance reaching a plateau for hundred processors and over. From the series of simulations, it seems that domain resolution and sub-catchment partitioning condition affect the performance. Other aspects such as initial landscape complexity and processes parametrisation might play an important role that will need further testing.

5. Delta evolution with sea-level change

5.1. Experimental settings

In this first example, we investigate the formation of river-dominated deltas under steady climatic conditions (uniform

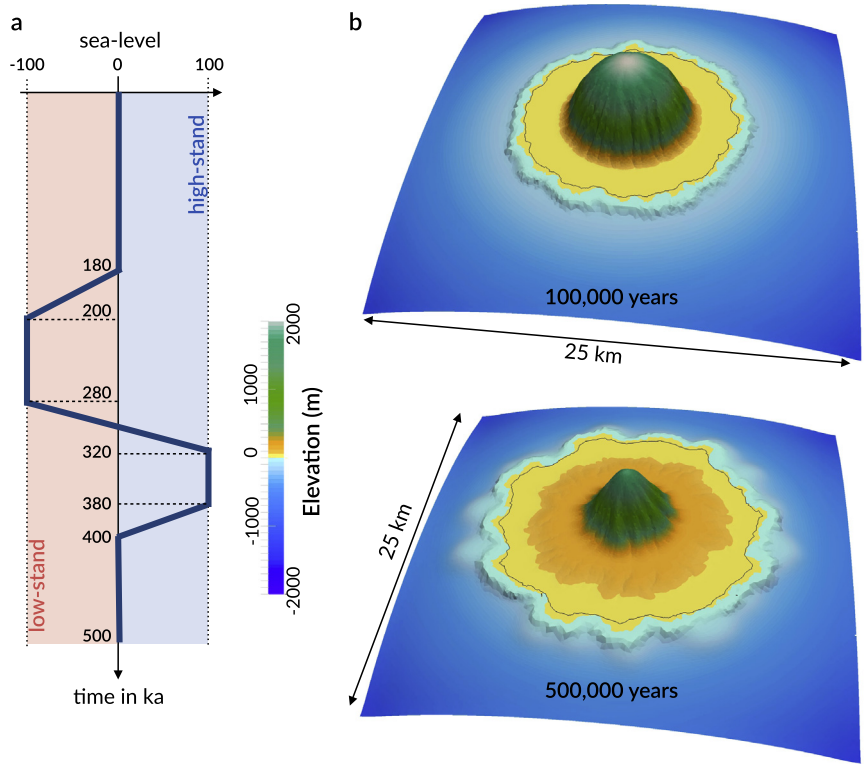

Fig. 7. (a) Imposed sea-level fluctuations for the experiment. (b) Perspective view of landscape evolution in time induced by the incision and diffusion laws for an artificial half ellipsoid mountain. The model shows the erosion of the mountain and the sedimentation front evolving after 100,000 years and at the end of the simulation.

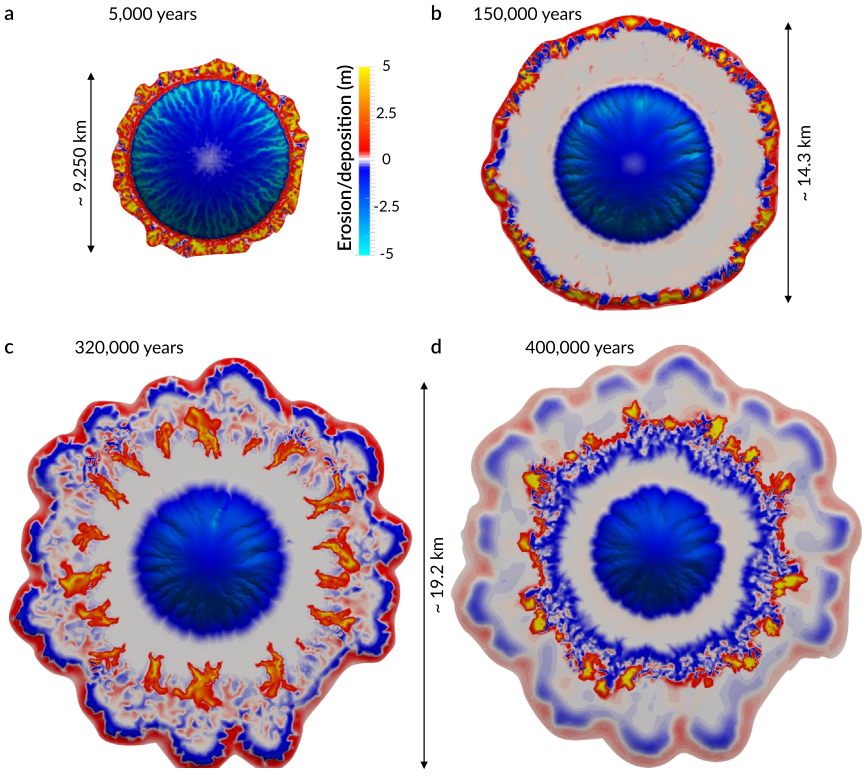

Fig. 8. Top views of the erosional and depositional patterns at 4 distinct times. The model shows a constant erosion of the mountain from (a) to (d) The evolution of the sedimentation area is more complex with progradation to deeper water in (a) and (b) and filling of incised valleys during transgression phases (c). Marine deposits propagate downslope due to higher diffusion coefficient as shown in (d).

precipitation) and sea-level fluctuations. Our goal is to reproduced first-order sea-level control on river deltas formation. This control has already been well established in the field of sedimentary geology, based on many field observations (Galloway, 1975; Wright, 1985; Catuneanu, 2006; Ainsworth et al., 2008) and numerical models (Stive and Vriend, 1995; Stolper et al., 2005;

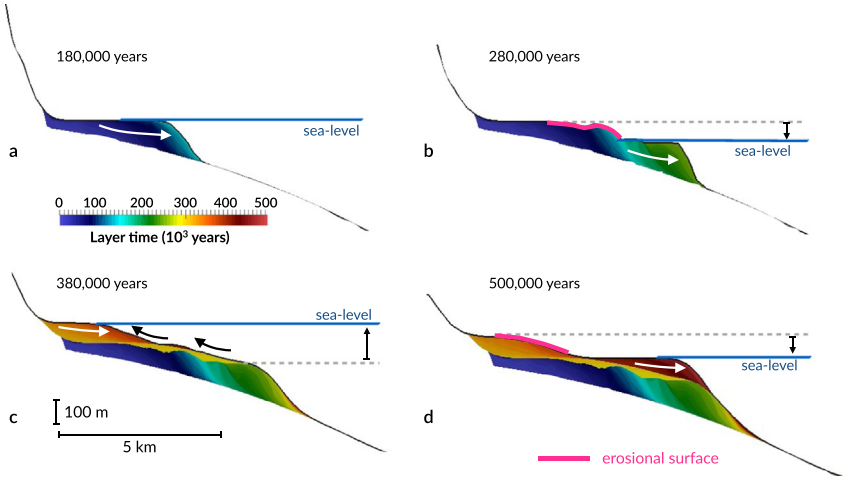

Fig. 9. Sequence stratigraphic evolution along a profile showing the successive progradation and transgression of the sedimentation due to sea-level change. Each section is coloured by time. As shown most of the time dependent deposits are preserved in the sedimentary sequences by the end of the simulation. (For interpretation of the references to colour in this figure caption, the reader is referred to the web version of this paper.)

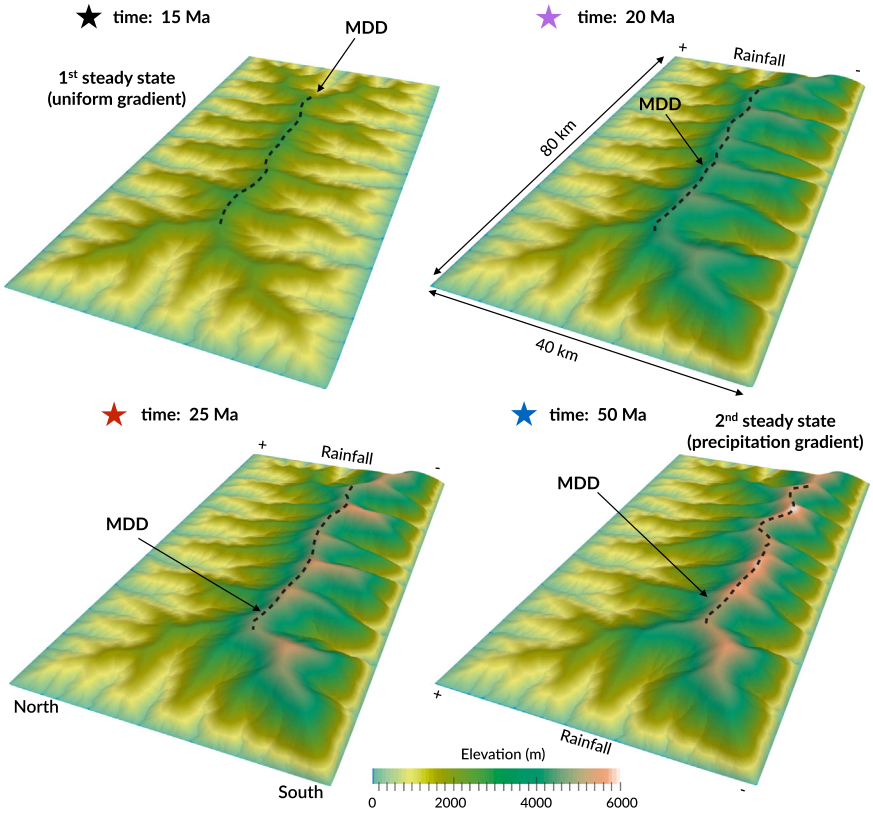

Fig. 10. Time evolution of a badlands model of block uplift under different precipitation climates showing the emergence of a mountain range and its drainage network. Panels are colour coded by elevation. The top left figure illustrates steady state under uniform precipitation and the next 3 figures the progressive evolution of the landscape under an orographic precipitation towards a second steady state (bottom right). The mean drainage divide (MDD) progressively migrates from the centre to the dryer side of the model area.

Swenson et al., 2005; Geleynse et al., 2010).

The initial surface defines a mount which is a half ellipsoid of 2 km height and a circular diameter of 8 km (Fig. 7b). The sea-level is initially set at the base of this mount at an elevation of 0 m. A uniform precipitation rate of 1 m/a is applied on the entire area and we test the evolution of the surface and associated deposits due to both hillslope and channel flow. The flexural isostasy is not considered in this example. Two diffusion coefficients are defined for the aerial (0.3 m^2/a) and marine (0.5 m^2/a) environments. The higher value for the marine environment is used to account for sediments reworking by waves or currents. The simulation runs for 0.5 Ma and we vary the sea-level through time (Fig. 7a). The initial grid is divided into two resolutions by defining a bounding box within the input file. A high-resolution area (mean triangle area: 10,000 m^2) is chosen around the mount, whereas the marine environment has a lower resolution (mean triangle area: 40,000 m^2).

5.2. Geomorphological evolution and sequence stratigraphy

During the first phase of the simulation, the mount is eroded and sediment are transported in the marine environment where

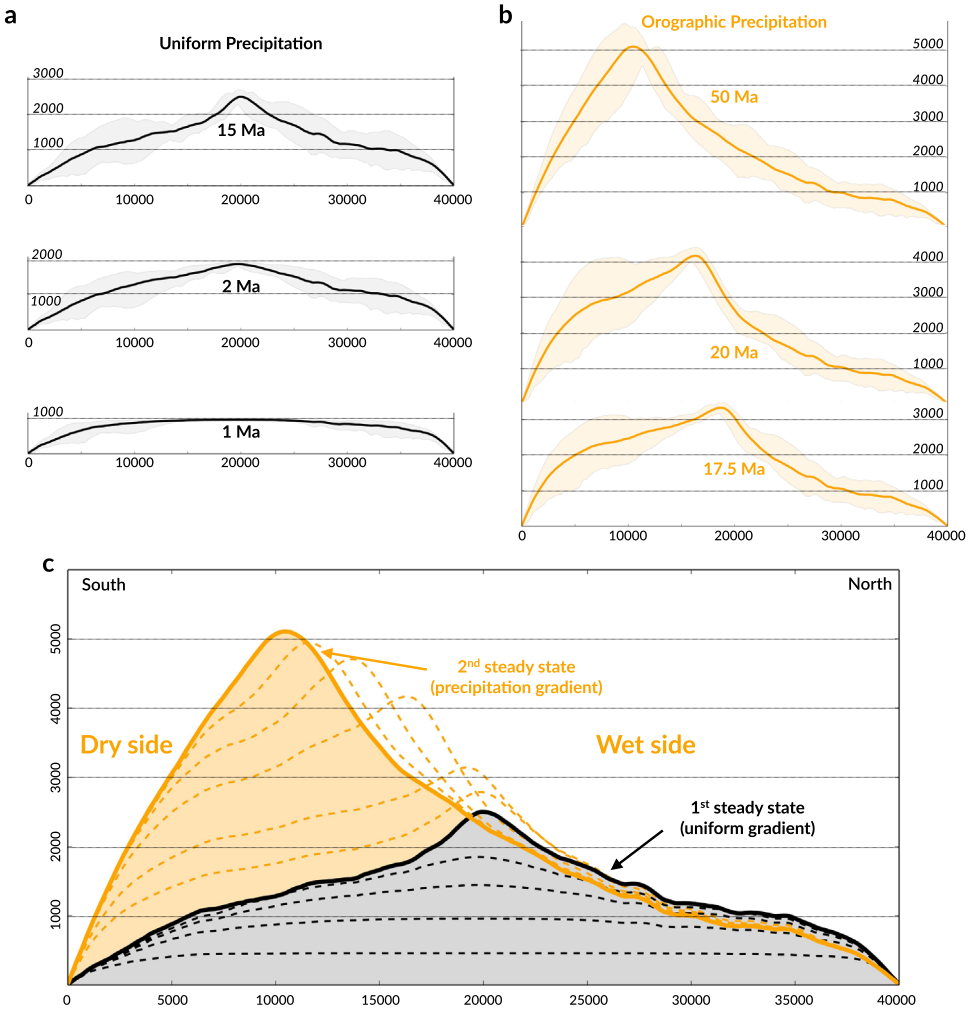

Fig. 11. Evolution of topographic profiles for 6 time intervals under the uniform and orographic precipitation climate (a & b); each line is the mean elevation along a North–South swath calculated from DEMs and is bounded by the minimum and maximum elevation range for each time steps. (c) Dotted and solid lines show evolution toward first and second steady states, respectively highlighting the impact of climatic forcing on mountain dynamic. Both vertical and horizontal axes are in metres.

we see a sedimentation front prograding (Fig. 8a and b). The progradation slows as the toeset of the delta progrades into continually deeper waters and as the delta front widens (Fig. 9a).

As the sea-level falls, it creates a condition of forced regression (Catuneanu, 2006), in which the coast is forced to build seaward. During the falling stage, rivers incise on what was formerly a marine shelf, forming incised valleys. These incised valleys tend to widen and grow landwards. After 280,000 years, the low-stand system marks the greatest extent of subaerial exposure and erosion. The simulated stratigraphy shows erosion of the top of the previous stratigraphic packages and a set of prograding sequences during low-stand condition (Fig. 9b).

As the relative sea-level rises between 280,000 and 320,000 years, it leads to a transgressive system. During this stage the previously incised valleys are filled with sediments as shown in Fig. 8c (finger-like red/yellow forms around the mount).

During high-stand (from 320,000 to 380,000 years), the sedimentary system turns from retrogradational stacking in the transgressive system to progradational stacking in the high-stand system (Fig. 9c). During this stage, the sediment supply to the shelve favours the development of progradational sequences that are deposited on top of the first prograding event.

During the last 100,000 years, the system returns to its original sea-level state which is marked by small incisions of formerly deposited high-stand marine shelf deposits and development of a new sedimentation front (Fig. 8d). The resulting stratigraphic sequences are built on top of the low-stand sequences (Fig. 9d).

6. Orogenic landscapes modelling

6.1. Experimental settings

This section presents the predictions of landscape evolution in response to two simple climatic scenarios: uniform and orographic precipitation. We investigate the drainage network dynamics and the steady-state fluvial patterns that emerge from an application of these climatic forcing mechanisms.

The first part of the scenario starts from a flat topography subjected to a constant and uniform rate of tectonic rock uplift (1 mm/a) and precipitation (1 m/a). The domain is rectangular and the four edges are kept at a constant base-level elevation. The area is a 40×80 km domain forming a triangular irregular network with an averaged cell area of 40,000 m^2. After 15 Ma, the second scenario is applied and consists in a linearly varying rainfall pattern corresponding to an orographic precipitation with the same uniform tectonic uplift rate. The Northern part of the domain is experiencing a 2 m/a precipitation rate and the Southern part is subject to a 0.1 m/a precipitation rate for the next 35 Ma. Other parameters of the simulation are kept constant and include the

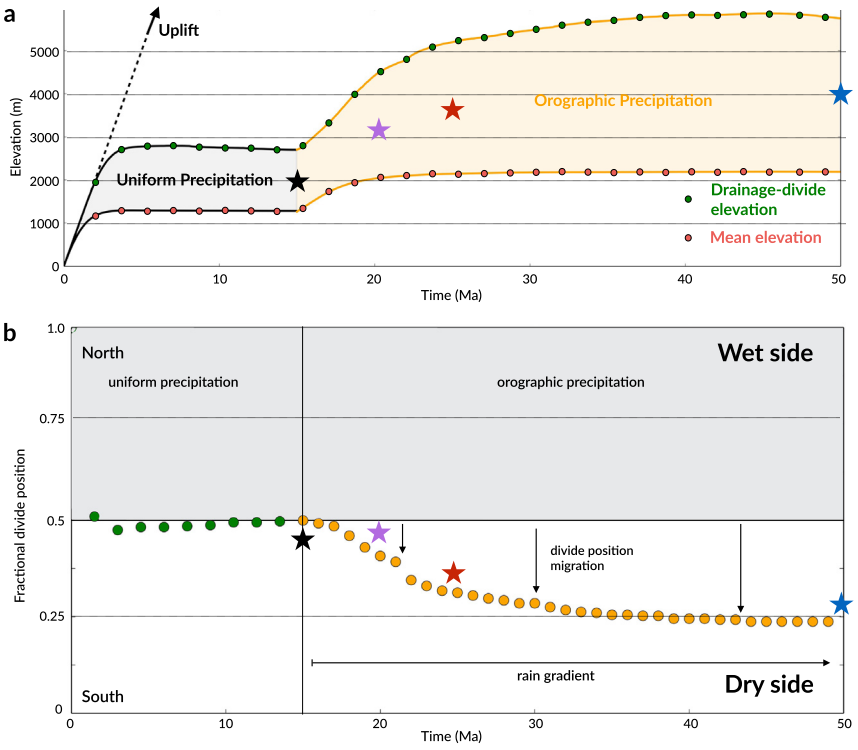

Fig. 12. (a) Evolution of mean and maximum (drainage-divide) elevations of the model. The dash line indicates the amount of applied uplift, that is, elevation of the model if no erosion occurred. The line is interrupted upward only for graphical convenience; uplift forcing was applied during the entire experiment at a constant rate. Note that the constancy of mean and maximum elevations after 4 Ma for the first evolution step implies a steady state between uplift and erosion. The second part of the graph under the orographic precipitation shows a similar trend with a mean elevation that reaches the steady-state after 25 Ma. The drainage-divide elevation shows however an increasing trend up to 36 Ma. (b) Evolution of the normalised divide position, highlighting the asymmetry development from the application of the rainfall gradient. After the precipitation gradient is applied, the main divide of the belt is pushed from the wet side towards the dry side. In both graphs coloured stars correspond to the time panels from Fig. 10. (For interpretation of the references to colour in this figure caption, the reader is referred to the web version of this paper.)

exponents $m=0.5$ and $n=1$ and the coefficients κ and ϵ which are set to 1.0 m^2/a and $5\times10^{-6}/a$ respectively.

6.2. Uniform precipitation scenario

First phase (Fig. 10 top left) shows the emergence of a mountain range with the main drainage divide subparallel to the long edges of the domain in response to block uplift conditions and uniform rainfall. The fluvial system that drains the mountain range develops gradually from the domain boundaries inward. Initially, the drainage network is composed of many small catchments that are formed by the steepest descent criterion that is used to compute drainage connectivity in badlands. Then, a plateau forms due to tectonic uplift. The edges of the plateau are eroded rapidly as incising channels propagate (Fig. 11a).

Eventually, a sub-linear mountain range is carved out of the plateau, with close to equally spaced main trunks (that reach the main divide draining it towards the four base-level edges (Fig. 10 top left). This phase is characterised by an increase in both the mean and maximum elevations (Fig. 12a).

After the growth phase, the mean and maximum elevations remain stable with time (Fig. 12a) even if local geometry evolves. A landscape is defined to be in topographical steady-state when every point in the landscape is statistically steady in elevation and the rate of tectonic rock uplift is exactly balanced by the rate of erosion (e.g., Montgomery, 2001; Willet and Brandon, 2002; Pelletier, 2004; Pelletier and Perron, 2012). Here, the mean elevation criterion is also used to define a steady state at the model scale. For the uniform precipitation scenario the landscape steady state is reached at around 5 Ma. Fig. 12b shows that the mean divide position for this phase is closely align with the centre of the domain which is consistent with analogue (Bonnet and Crave, 2003; Bonnet, 2009) and numerical (Willett et al., 2001; Kooi and Beaumont, 2006; Whipple, 2009; Goren et al., 2014) experiments.

6.3. Orographic precipitation scenario

Application of the orographic precipitation induces migration of the drainage divide towards the drier side of the landscape and development of an asymmetric topography (Figs. 10 and 12b), a response previously observed numerically (Roe et al., 2003; Anders et al., 2008) and experimentally (Bonnet, 2009).

In response to the precipitation gradient, the migration of the drainage divide induces a continuous decrease in the drainage area within the catchments located on the dryer side of the landscape. In the model, the drainage area is directly related to the water discharge and so is the sediment transport rate. As a consequence, the decrease of the drainage catchments size correlates with a steepening of their channels and of the overall relief in the South (Fig. 13b). Therefore, by reducing the discharge within drainage catchments, divide migration drives a narrowing of the channels so erosion is progressively localised within the floodplains, resulting in an overall uplift of the dryer side (Figs. 10 and 11b).

The slope of the profiles (Fig. 11b and c) for the northern and southern drainage indicates very contrasting evolutions. Landscape adjustment to the climate forcing takes more time than the growth phase for the uniform scenario. From Fig. 12a, the model requires around 10 Ma to reach a stage where the mean elevation remains stable with time. Thus for the second scenario the landscape steady state is reached at around 25 Ma but the drainage divide elevation and position still evolve up to 36 Ma (Figs. 11c and 12b).

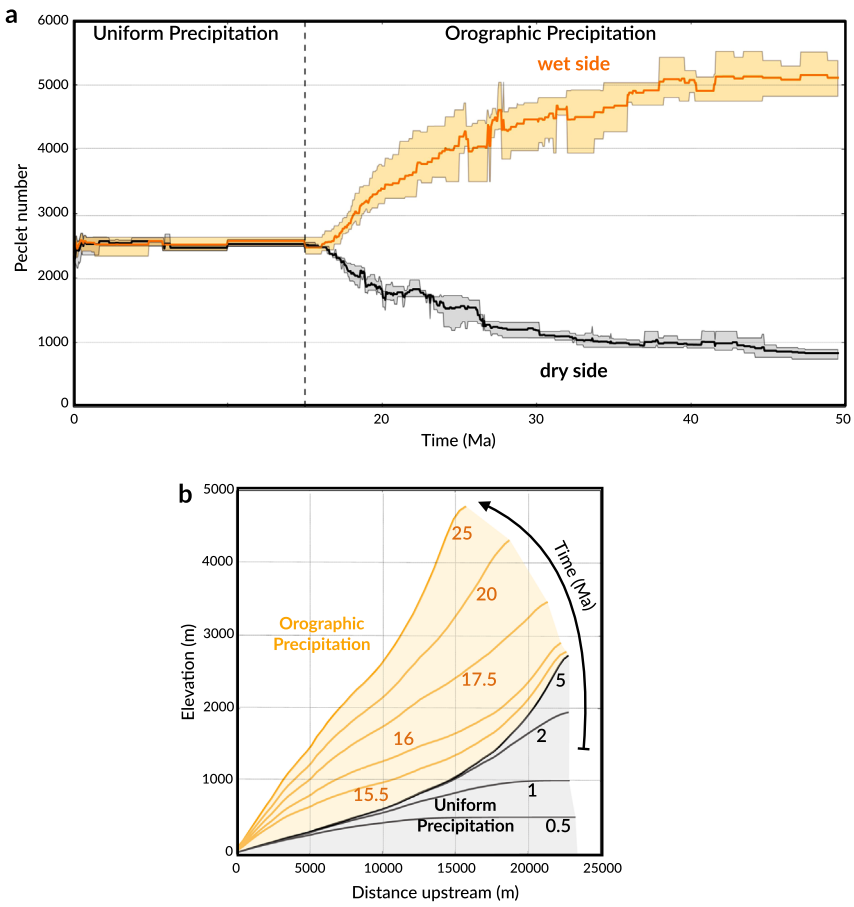

Fig. 13. (a) Time evolution of the mean Peclet number for the wet side (orange line) and the dry side (black line) of the simulated surface. In addition to the mean, the minimum and maximum range of calculated Peclet number is also given. (b) Time evolution of the longitudinal profile of the main channel in the dry side of the model (southern side). The stack of longitudinal profiles within the grey area corresponds to the evolution up to the steady state for the uniform precipitation scenario. In the orange area, the progressive shortening and steepening of the channel are linked to the orographic precipitation. (For interpretation of the references to colour in this figure caption, the reader is referred to the web version of this paper.)

6.4. *Drainage network reorganisation*

In Fig. 13a, we evaluate over time the dominant processes shaping the landscape based on the Peclet number *Pe* which captures the relative vigour of advective channel processes, represented by the coefficient ϵ, and diffusive hillslope processes, represented by κ (Birnir et al., 2001; Perron et al., 2009). We use the formulation from Giachetta et al. (2012):

$$Pe = \frac{\epsilon l^{2(m+1)-n}}{\kappa \eta^n}$$

where l is the distance from the valley outlet to the drainage divide and η the elevation of the drainage divide. As shown in Fig. 13a, the Peclet number curves for both sides of the model are similar under the uniform precipitation and diverge under the orographic condition. On the wet side where *Pe* is large, stream incision dominates and the landscape shows extensive valley networks and small hillslopes. Conversely, on the dry side *Pe* is significantly smaller (by a factor 5 at 50 Ma), stream incision dominates erosion over a reduced fraction of the terrain, hillslopes are larger and the valley network is less extensive. The simulation shows that the extent of valley incision is set by a balance between diffusive hillslope processes and advective channel processes. As suggested by Sweeney et al. (2015) experiments, perturbations to this process-rate balance, driven by changes in climate, is changing the reach of erosional valley networks.

During the first scenario (uniform precipitation), channel profiles evolve symmetrically on both sides of the model. By the time the first steady state is reached (approximately 5 Ma), all the channels have developed a characteristic concave up shape (Zaprowski et al., 2005) as illustrated in Fig. 13b. Then, the imposed orographic precipitation is driving an abrupt change in the channels gradient for the dry side of the model. The channels continuously steepen as they shorten because of divide migration. By 25 Ma, channels from the dry side have reached their steepest gradients which are mainly controlled by hillslope processes (*i.e* κ coefficient). The landscape at this point has reached a second steady state.

Landscape dynamics and network organisation from our simulation and the quantitative interpretations presented above are in agreement with recent studies using analogue and numerical models (Willett, 1999; Bonnet, 2009; Perron et al., 2009; Giachetta et al., 2012). The model also shows analogies between the synthetic landscapes extracted from the numerical simulation and real landscapes with similar tectonic and climatic conditions such as the *Ruby Mountains, USA* (Ellis et al., 1999) or the *Sierra Aconquija, Argentina* (Bonnet, 2009).

7. Conclusion

Badlands is an open source tool for the simulation of catchment and landscape dynamics that integrates a minimal set of well established physical laws. The model is capable of simulating

hillslope processes (diffusion law), fluvial erosion (stream power law), sediment transport (sediment flux conservation) and deposition (in depression areas) as well as isostatic flexure on heterogeneous lithosphere. The model can be used to quantify the geomorphic and sedimentary response to spatially and temporally varying tectonic and climatic forces (precipitation and sea-level).

A finite volume approach, based on the dual Delaunay–Voronoi framework, is used to solve the continuity equation explicitly. The numerical solution stability is ensured by a CFL-like condition. The model is designed to serve as a general-purpose framework for investigating a range of problems in drainage and sedimentary basin geomorphology, with an emphasis on morphological development. The model efficiency comes from (1) a $O(n)$-efficient ordering method and (2) a sub-catchments partitioning approach which minimises inter processor communications and balances the computational load among processors.

In this paper, we illustrate the model with two examples. First we simulate the evolution of a deltaic system under sea-level fluctuations. The model is able to reproduce the successive phases of progradation and transgression and the associated stratigraphic sequences. Then the model is used to quantify the importance of climate change on the formation of mountain belts. The numerical results and quantitative analyses show that change in precipitation pattern exerts a strong control on drainage catchments evolution and networks reorganisation on both sides of the mountain belt as the main drainage divide migrates. The model results are in agreement with recent studies based on natural, analogue and numerical models.

Badlands source code, the associated documentation along with a series of examples are available on Github (http://github.com/badlands-model).

References

Ainsworth, R.B., Flint, S.S., Howell, J.A., 2008. Predicting coastal depositional style: influence of basin morphology and accommodation to sediment supply ratio within a sequence-stratigraphic framework. In: Hampson, G.J., Steel, R.J., Burgess, P.M., Dalrymple, R.W. (Eds.), Recent Advances in Models of Shallow-Marine Stratigraphy: SEPM Special Publication, vol. 90. pp. 237–263.

Altas, I., Dym, J., Gupta, M., Manohar, R.P., 1998. Multigrid solution of automatically generated high-order discretizations for the biharmonic equation. SIAM J. Sci. Comput. 19, 1575–1585.

Anders, A.M., Roe, G.H., Montgomery, D.R., Hallet, B., 2008. Influence of precipitation phase on the form of mountain ranges. Geology 36, 479–482.

Arnold, J.G., Srinivasan, R., Muttiah, R.S., Williams, J.R., 1998. Large area hydrologic modeling and assessment—Part 1: model development. J. Am. Water Resour. Assoc. 34 (1), 73–89.

Birnir, B., Smith, T., Merchant, G.E., 2001. The scaling of fluvial landscapes. Comput. Geosci. 27, 1189–1216.

Bonnet, S., Crave, A., 2003. Landscape response to climate change: insights from experimental modeling and implications for tectonic versus climatic uplift of topography. Geology 31, 123–126.

Bonnet, S., 2009. Shrinking and splitting of drainage basins in orogenic landscapes from the migration of the main drainage divide. Nat. Geosci. 2, 766–771.

Braun, J., Heimsath, A.M., Chappell, J., 2001. Sediment transport mechanisms on soil-mantled hillslopes. Geology 29 (8), 683–686.

Braun, J., Sambridge, M., 1997. Modelling landscape evolution on geological time scales: a new method based on irregular spatial discretization. Basin Res. 9 (1), 27–52.

Braun, J., Willett, S.D., 2013. A very efficient O(n), implicit and parallel method to solve the stream power equation governing fluvial incision and landscape evolution. Geomorphology 180, 170–179.

Catuneanu, O., 2006. Principles of Sequence Stratigraphy. Elsevier, Amsterdam, p. 375.

Chen, A., Darbon, J., Morel, J.M., 2014. Landscape evolution models: a review of their fundamental equations. Geomorphology 219, 68–86.

Coulthard, T.J., 2001. Landscape evolution models: a software review. Hydrol. Process. 15, 165–173.

Delaunay, J., 1934. Sur la sphère vide. A la mémoire de Georges Voronoï. Bulletin de l'Académie des Sciences de l'URSS. Cl. Sci. Math. 6, 793–800.

Dietrich, W.E., Reiss, R., Hsu, M.L., Montgomery, D.R., 1995. A process-based model for colluvial soil depth and shallow landsliding using digital elevation data. Hydrol. Process. 9 (3–4), 383–400.

Ellis, M., Densmore, A.L., Anderson, R.S., 1999. Development of mountainous topography in the Basin Ranges, USA. Basin Res. 11, 21–41.

Fernandes, N., Dietrich, W.E., 1997. Hillslope evolution by diffusive processes: the timescale for equilibrium adjustments. Water Resour. Res. 33 (6), 1307–1318.

Gallant, J., Wilson, J., 2000. Primary terrain attributes. In: Wilson, J., Gallant, J. (Eds.), Terrain Analysis: Principles and Applications. John Wiley and Sons, New York, pp. 51–85.

Galloway, W.E., 1975. Process framework for describing the morphologic and stratigraphic evolution of deltaic depositional systems. In: Broussard, M.L. (Ed.), Deltas: Models for Exploration. Houston Geological Society, Houston, TX, pp. 87–98.

Garcia-Castellanos, D., Vergés, J., Gaspar-Escribano, J.M., Cloetingh, S., 2003. Interplay between tectonics, climate and fluvial transport during the Cenozoic evolution of the Ebro Basin (NE Iberia). J. Geophys. Res. 108 (B7), 2347.

Geleynse, N., Storms, J.E.A., Stive, M.J.F., Jagers, H.R.A., Walstra, D.J.R., 2010. Modeling of a mixed-load fluvio-deltaic system. Geophys. Res. Lett. 37, L05402.

Giachetta E., Gasparini, N., Capolongo, D., Refice, A., Pazzaglia, F.J., 2012. The role of climate change in drainage network reorganization: insights from numerical experiments. EGU Geophysical Research Abstracts, vol. 14, EGU2012-7438.

Goren, L., Willett, S.D., Herman, F., Braun, J., 2014. Coupled numerical-analytical approach to landscape evolution modeling. Earth Surf. Process. Landforms 39, 522–545. http://dx.doi.org/10.1002/esp.3514.

Gropp, W., Lusk, E., Skjellum, A., 1999. Using MPI: Portable Parallel Programming with the Message-Passing Interface. MIT Press, Cambridge, MA.

Karypis, G., Kumar, V., 1999. A fast and high quality multilevel scheme for partitioning irregular graphs. SIAM J. Sci. Comput. 20 (1), 359–392.

Kooi, H., Beaumont, C., 2006. Large-scale geomorphology: classical concepts reconciled and integrated with contemporary ideas via a surface process model. J. Geophys. Res. 101 (B2), 3361–3386.

Lague, D., Hovius, N., Davy, P., 2005. Discharge, discharge variability, and the bedrock channel profile. J. Geophys. Res. 110, 1–17.

Li, F., Dyt, C., Griffiths, C., 2004. 3D modelling of flexural isostatic deformation. Comput. Geosci. 30 (9), 1105–1115.

Howard, A., 1980. Thresholds in river regimes. In: Coates, D.R., Vitek, J.D. (Eds.), Thresholds in Geomorphology. George Allen & Unwin, London, pp. 227–258.

Montgomery, D.R., 2001. Slope distributions, threshold hillslopes, and steady-state topography. Am. J. Sci. 301, 432–454.

O'Callaghan, J., Mark, D., 1984. The extraction of drainage networks from digital elevation data. Comput. Vis. Graph. Image Process. 28, 323–344.

Paola, C., Straub, K., Mohrig, D., Reinhardt, L., 2009. The unreasonable effectiveness of stratigraphic and geomorphic experiments. Earth-Sci. Rev. 97 (1–4), 1–43.

Pelletier, J., 2004. Persistent drainage migration in a numerical landscape evolution model. Geophys. Res. Lett. 31 (L20501), 2004.

Pelletier, J.D., Perron, J.T., 2012. Analytic solution for the morphology of a soil-mantled valley undergoing steady headward growth: validation using case studies in southeastern Arizona. J. Geophys. Res. 117, F02018. http://dx.doi.org/10.1029/2011JF002281.

Perron, J.T., Kirchner, J.W., Dietrich, W.E., 2009. Formation of evenly spaced ridges and valleys. Nature 460, 502–505.

Refice, A., Giachetta, E., Capolongo, D., 2012. SIGNUM: a Matlab, TIN-based landscape evolution model. Comput. Geosci. 45, 293–303.

Roe, G.H., Montgomery, D.R., Hallet, B., 2003. Orographic precipitation and the relief of mountain ranges. J. Geophys. Res. 108, 2315.

Salles, T., Duclaux, G., 2015. Combined hillslope diffusion and sediment transport simulation applied to landscape dynamics modelling. Earth Surf. Process. Landforms 40 (6), 823–839.

Shewchuk, J.R., 2002. Delaunay refinement algorithms for triangular mesh generation. Comput. Geom.: Theory Appl. 22 (1–3), 21–74.

Slingerland, R., Harbaugh, J.W., Furlong, K.P., 1994. Simulating Clastic Sedimentary Basins. PTR Prentice-Hall, Englewood Cliffs, NJ, p. 220.

Stive, M.J.F., Vriend, H.J.De., 1995. Modelling shoreface profile evolution. Mar. Geol. 126, 235–248.

Stolper, D., List, J.H., Thieler, R.E., 2005. Simulating the evolution of coastal morphology and stratigraphy with a new morphological-behaviour model (GEOMBEST). Mar. Geol. 1 (4), 17–36.

Strahler, A.N., 1952. Hypsometric (area-altitude) analysis of erosional topology. Geol. Soc. Am. Bull. 63 (11), 1117–1142.

Sweeney, K.E., Roering, J.J., Ellis, C., 2015. Experimental evidence for hillslope control of landscape scale. Science 349, 51.

Swenson, J.B., Paola, C., Pratson, L., Voller, V.R., Murray, A.B., 2005. Fluvial and marine controls on combined subaerial and subaqueous delta progradation: morphodynamic modeling of compound-clinoform development. J. Geophys. Res. 110, F02013.

Tucker, G.E., 2009. Natural experiments in landscape evolution. Earth Surf. Process. Landforms 34 (10), 1450–1460.

Tucker, G.E., Hancock, G.R., 2010. Modelling landscape evolution. Earth Surf. Process. Landforms 35 (1), 28–50.

Tucker, G.E., Lancaster, S.T., Gasparini, N.M., 2001. The channel-hillslope integrated landscape development (CHILD) model. In: Harmon, R.S., Doe, W. (Eds.), Landscape Erosion and Evolution Modeling, 3rd edition Kluwer Academic/Plenum, New York, pp. 349–388 (Chapter 12).

Vivoni, E.R., Mascaro, G., Mniszewski, S., Fasel, P., Springer, E.P., Ivanov, V.Y., Bras, R.L., 2011. Real-world hydrologic assessment of a fully-distributed hydrological model in a parallel computing environment. J. Hydrol. 409, 483–496.

Voronoi, G., 1908. Nouvelles applications des paramètres continus à la théorie de formes quadratiques. J. Reine Angew. Math. 134, 198–287.

Whipple, K., Tucker, G.E., 1999. Dynamics of the stream-power river incision

model: implications for height limits of mountain ranges, landscape response timescales, and research needs. J. Geophys. Res. 104 (B8), 17661–17674.
Whipple, K., 2009. The influence of climate on the tectonic evolution of mountain belts. Nat. Geosci. 2, 97–104.
Wickert, A.D., 2015. Open-source modular solutions for flexural isostasy: gFlex v1.0. Geosci. Model Dev. Discuss. 8, 4245–4292.
Willett, S.D., 1999. Orogeny and orography: the effects of erosion on the structure of mountain belts. J. Geophys. Res. 104 (B12), 28957–28981.
Willett, S.D., Slingerland, R., Hovius, N., 2001. Uplift, shortening, and steady-state in active mountain belts. Am. J. Sci 301, 455–485.
Willet, S.D., Brandon, M.T., 2002. On steady states in mountain belts. Geology 30, 175–178.
Willgoose, G., 2005. Mathematical modeling of whole landscape evolution. Annu. Rev. Earth Planet. Sci. 33 (1), 443–459.
Wright, L.D., 1985. River deltas. In: Davis, R.A. (Ed.), Coastal Sedimentary Environments. Springer-Verlag, New York, pp. 1–76.
Zaprowski, B.J., Pazzaglia, F.J., Evenson, E.B., 2005. Climatic influences on profile concavity and river incision. J. Geophys. Res. 110, F03004. http://dx.doi.org/10.1029/2004JF000138.